

# Noise, transient dynamics, and the generation of realistic interspike interval variation in square-wave burster neurons

Bóris Marin<sup>\*</sup>

*Instituto de Física, Universidade de São Paulo, Brazil<sup>†</sup>*

Reynaldo Daniel Pinto<sup>‡</sup>

*Instituto de Física de São Carlos, Universidade de São Paulo, Brazil*

Robert C. Elson<sup>§</sup>

*Institute for Nonlinear Science, University of California, San Diego, CA 92093-0402, USA<sup>¶</sup>*

Eduardo Colli<sup>\*\*</sup>

*Instituto de Matemática e Estatística, Universidade de São Paulo, Brazil*

(Dated: July 4, 2014)

## Abstract

First return maps of interspike intervals for biological neurons that generate repetitive bursts of impulses can display stereotyped structures (neuronal signatures). Such structures have been linked to the possibility of multicoding and multifunctionality in neural networks that produce and control rhythmical motor patterns. In some cases, isolating the neurons from their synaptic network reveals irregular, complex signatures that have been regarded as evidence of intrinsic, chaotic behavior.

We show that incorporation of dynamical noise into minimal neuron models of square-wave bursting (either conductance-based or abstract) produces signatures akin to those observed in biological examples, without the need for fine-tuning of parameters or ad hoc constructions for inducing chaotic activity. The form of the stochastic term is not strongly constrained, and can approximate several possible sources of noise, e.g. random channel gating or synaptic bombardment.

The cornerstone of this signature generation mechanism is the rich, transient, but deterministic dynamics inherent in the square-wave (saddle-node/homoclinic) mode of neuronal bursting. We show that noise causes the dynamics to populate a complex transient scaffolding or skeleton in state space, even for models that (without added noise) generate only periodic activity (whether in bursting or tonic spiking mode).

PACS numbers: 87.19.lc

---

\* bmarin@if.usp.br

† Present address: Department of Neuroscience, Physiology and Pharmacology, University College London, London, UK

‡ reynaldo@ifsc.usp.br

§ RobertElson@pointloma.edu

¶ Present address: Department of Biology, Point Loma Nazarene University, San Diego, CA 92106, USA

\*\* colli@ime.usp.br

## I. INTRODUCTION

First return maps of interspike intervals (ISIs) of bursting biological neurons reveal characteristic patterns of firing sequences [1–4]. In invertebrate central pattern generators (CPGs) [1, 2], ISI return maps consist of a specific arrangement of clusters, called a neuronal signature [1, 2]. The reproducibility of these signatures allows the identification of neuronal types in circuits presenting different bursting frequencies, duty cycles and number of spikes per burst, even across biological species [5]. Moreover, the signature reflects circuit connectivity [1, 2], information in synaptic input patterns [5] and the modulation of network operation [6].

In realistic electrophysiological neuronal models, several dynamical variables and parameters interact in nonlinear ways to produce complex activity patterns, such as quiescence, tonic spiking and bursting. The spiking-bursting activity may be periodic or chaotic. A burst of spikes, taken as a whole, might function as a robust unit of neural information [7–10]. In contrast, the possibility of information coding *within* bursts has received little attention.

The information-processing properties of CPGs have been explored in model circuits inspired by the networks in the crustacean stomatogastric ganglion (STG) [11–13]. The authors proposed a CPG that generates a steady rhythm of bursts but also responds to or recognizes the signatures produced by its individual neurons. Analysis in the STG has shown that there is a neuron-to-neuron flow of information within a bursting, rhythm-generating network [5].

The ISI return maps of many STG neurons change considerably when the cells are disconnected from their synaptic circuit. In these isolated neurons, the ISI sequences *within* each burst vary *between* bursts, this variation growing exponentially as bursts evolve and the spike train progresses [14]. This activity has been classified as chaotic bursting [15]. The neurophysiological mechanisms of this behavior have remained elusive. Detailed, conductance-based models generally produce regular activity when parameters are set to biologically plausible values [16]. Deterministic neuron models operating in chaotic regimes can generate irregular (non-periodic, broad spectrum) time-series, but their ISI return maps are highly structured, because chaotic trajectories are confined to particular regions of state space [17–20]. Moreover, the production of chaotic activity involves fine-tuning of model parameters in order to meet strict criteria, e.g. being close to spike-adding bifurcations [19].

In contrast, state-space trajectories generated by stochastic processes are not confined in

this way, because noise is able to nudge a dynamical system to populate the transient scaffolding (skeleton) inherent in the dynamics. Accordingly, we here propose a mechanism to generate the ISI signature of irregularly bursting neurons based on the interplay of deterministic and stochastic dynamics. The noiseless system does not need to be tuned to a chaotic regime, nor is there a restrictive definition of the origin of the noise. We anticipate that this approach can be applied to other problems as well, such as burst alignment algorithms and noise-level estimation.

## II. METHODS

### A. Biological neurons: recordings and analysis

The stomatogastric nervous system was removed from spiny lobsters, *Panulirus interruptus*, and pinned out in vitro in standard *Panulirus* saline [14]. The STG, which contains the rhythm-generating pyloric circuit, remained connected to anterior ganglia whose descending modulatory influence sustain cellular bursting activity. The lateral pyloric LP or a pyloric dilator neuron PD neuron were disconnected from synaptic input from other pyloric circuit neurons by photoinactivating or deeply hyperpolarizing some presynaptic neurons and blocking inputs from others pharmacologically [21, 22]. After synaptic isolation, neurons were impaled by two microelectrodes for independent current injection and membrane potential recording.

Signature maps were obtained by detecting spikes via crossing a threshold of  $-35\text{mV}$ . After each such crossing, new spike detection was allowed only after the membrane potential timeseries crossed a reset threshold of  $-38\text{mV}$ .

### B. Neuron Model

Our analysis made use of a tridimensional conductance-based neuronal model (1). This model has been introduced as a minimal model for square-wave bursting [23] and has been previously analyzed in [20, 24]. It consists of a two-dimensional fast subsystem coupled to a one-dimensional slower one. The fast subsystem consists of a persistent sodium current with instantaneous activation  $I_{\text{Nap}}$ , and a potassium current  $I_{\text{Kd}}$ . The slow subsystem comprises

the gating dynamic of an *M-type* potassium current  $I_{\text{KM}}$ . The biophysical parameters are listed in table I.

$$C\dot{V} = I_{\text{ext}} - g_{\text{leak}}(V - V_{\text{leak}}) - \overbrace{\bar{g}_{\text{Nap}} m_{\text{Nap}}^{\infty} (V - V_{\text{Nap}})}^{I_{\text{Nap}}} - \underbrace{\bar{g}_i m_i (V - V_{\text{K}})}_{I_i} \quad (1)$$

$$\dot{m}_i = \frac{m_i^{\infty} - m_i}{\tau_i} \quad i = [\text{Kd}, \text{KM}]$$

TABLE I. Parameters for the currents in the deterministic simulations (equation 1).  $V_i$  are the ionic reversal potentials,  $\bar{g}_i$  are maximum conductance densities,  $\tau_i$  are the timescales for each conductance. The steady state activation functions are defined as  $m_i^{\infty} = \{1 + \exp[(V_i^{1/2} - V)/k_i]\}^{-1}$ , where  $V$  stands for the membrane potential. Other passive parameters are the membrane specific capacitance  $C = 1 \mu\text{Fcm}^{-2}$  and a DC bias  $I_{\text{ext}} = 5 \mu\text{Acm}^{-2}$ .

	Nap	Kd	KM	leak
$V_i$ (mV)	60	-90	-90	-80
$\bar{g}_i$ (mS cm $^{-2}$ )	20	9	5	8
$V_i^{1/2}$ (mV)	-19.9	-25	-21.2	—
$k_i$ (mV)	15	5	5	—
$\tau_i$ (ms)	—	0.152	20	—

Bursting activity is generated via an hysteretic loop. It can be easily analyzed by considering the slow variable  $m_{\text{KM}}$  as a bifurcation parameter [23, 25], which drives the fast subsystem cyclically from a branch of equilibria (henceforth denoted as  $\mathcal{E}$ ) to a limit cycle manifold  $\mathcal{L}$  (Fig. 1). When the trajectory (gray curve in Fig. 1) slides along the stable equilibrium part of  $\mathcal{E}$  (solid segment of blue line marked as  $\mathcal{E}$ ), the full tridimensional system is in the hyperpolarized, interburst phase. Since the flux is evolving below the  $m_{\text{KM}}$  nullcline (red curve), it moves toward smaller  $m_{\text{KM}}$  values. The stable equilibrium eventually loses stability in a saddle-node bifurcation (point labeled SN), so the trajectory moves towards the spiking manifold  $\mathcal{L}$  (black “tube”). Crossing the  $m_{\text{KM}}$  nullcline leads the trajectories to move towards larger  $m_{\text{KM}}$  values. Spikes in the active phase of bursting correspond to full revolutions around  $\mathcal{L}$ . This manifold disappears in a saddle-homoclinic orbit bifurcation (point labelled S-H), when it collides with the middle (saddle) segment of  $\mathcal{E}$ .

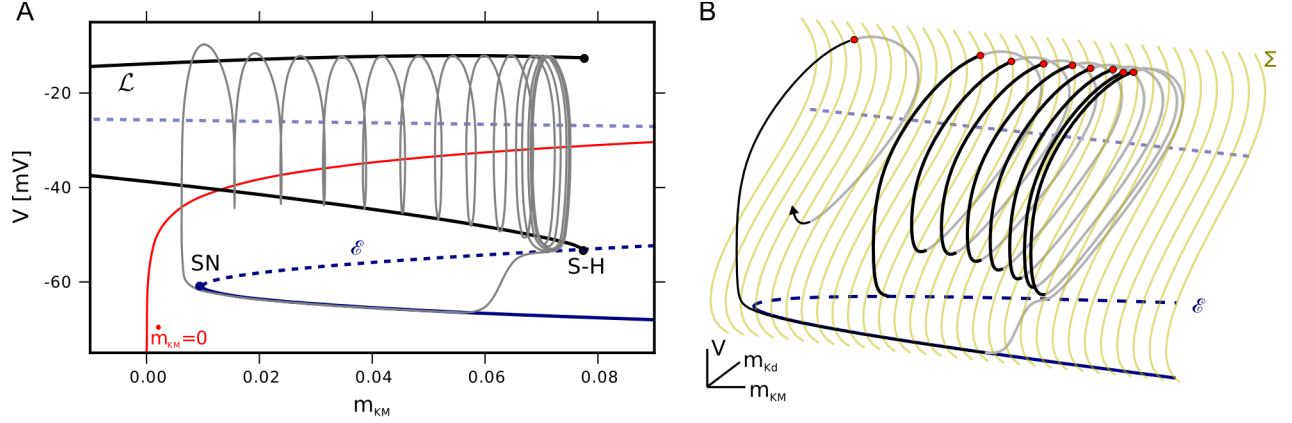


FIG. 1. A: Phase portrait for the noiseless neuronal model (eq. 1). A noiseless bursting trajectory is depicted in gray. The blue curves correspond to the fast subsystem equilibrium branch  $\mathcal{E}$ , where solid/dashed lines denote stable/unstable(saddle) states. The black “tube” depicts the spiking manifold  $\mathcal{L}$ . The red curve is the  $m_{\text{KM}}$  nullcline: trajectories below(above) it move towards smaller(larger)  $m_{\text{KM}}$  values. Labelled points indicate bifurcations in the fast subsystem: SN: saddle-node and S-H: saddle – homoclinic orbit. B: Full-model trajectory (black / gray curve) emanating from initial condition in the unstable manifold of the saddle branch  $\mathcal{E}$ . The Poincaré surface of section  $\Sigma$  is depicted in beige. Red points represent  $\Sigma$  crossings, used in the reduced model analysis.

Several conductance-based models can give rise to square-wave bursting, including those built to study systems as diverse as pancreatic  $\beta$ -cells [19, 26], neurons in the pre-Bötzinger complex of the brain stem [27, 28] or hippocampal CA1 pyramidal cells [29]. Our analysis can be applied to any of these or even other systems, provided that bursting involves a saddle middle branch in the equilibrium curve of the fast subsystem.

As additional examples of square-wave bursting neuron signatures, we have included those generated by the Hindmarsh-Rose three dimensional model [30], with parameters as in table II, and a model for neurons in the pre-Bötzinger complex (model and parameters described

TABLE II. Parameter values for the Hindmarsh-Rose neuron model, periodic bursting mode.

$a$	$b$	$c$	$d$	$s$	$x_1$	$r$	$I$
1	2.7	1	5	4	-1.6	0.01	4

in [27], model 1). In both models, the chosen parameter set supported periodic bursting

activity.

### C. Stochastic dynamics

Stochastic ion channel gating has been suggested to be the major source of noise in isolated neurons [31]. Since our derivation of the generative model for ISI map signatures does not impose constraints nor require a particular noise mechanism, we chose to model stochastic gating using three different approaches [32]. For the Nap-Kd-KM model, we used a Langevin approximation to microscopic gating schemes derived in [33]. In this approximation, the subunit gating dynamics  $\dot{m}_i$  are complemented with a state dependent (multiplicative) random forcing  $\xi$ , with zero mean and variance inversely proportional to the number of channels  $N$  in the membrane patch, according to equation 2.

$$\begin{aligned}\dot{m}_i &= \frac{m_i^\infty - m_i}{\tau_i} + \xi_i & \langle \xi_i \rangle &= 0 \\ \langle \xi_i(t) \xi_i(t') \rangle &= \frac{m_i^\infty(1 - m_i^\infty)}{N_i \tau_i} \delta(t - t')\end{aligned}\tag{2}$$

For the Hindmarsh-Rose model, we opted for the current noise approach [32], adding a stochastic force directly to the membrane potential equation. Finally, for the pre-Bötzinger neuron model, we used conductance noise [32, 33], where the stochastic terms are added to the conductance terms in the voltage dynamics:  $I_i = \bar{g}_i(m_i + \xi_i)(V - V_i)$ .

The resulting stochastic differential equations were integrated numerically, using the Euler-Maruyama scheme [34] with a fixed timestep of 0.001 ms.

## III. RESULTS

### A. ISI maps of irregular bursting in biological neurons

The biological neurons, LP and PD, generated irregular spiking-bursting activity of the type shown by the excerpted time-series in Fig. 4C. Maps of the ISIs for spike trains within bursts are shown in the boxed areas of Fig. 2. The initial ISIs, from the start of bursts, are shown in panels A2, B2. As the bursts evolve, the dispersion of corresponding sequential ISIs increases greatly. Bursts also vary in total number of spikes.

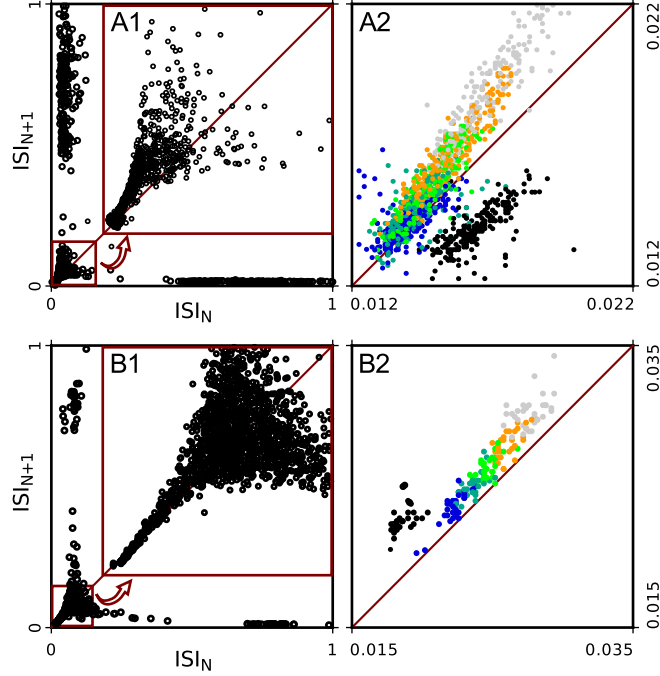


FIG. 2. First return ISI maps for bursting activity of isolated LP(A) and PD(B) neurons from the STG of the lobster *Panulirus interruptus*. Colours (A2, B2) indicate successive ISI pairs at the start of bursts. ISI have been normalized so that  $\max(\text{ISI}) = 1$ .

## B. Unidimensional reductions of neuronal model

We now construct a hybrid (deterministic/stochastic) mechanism for generating ISI map signatures similar to those of biological neurons. It is convenient to start with unidimensional reductions of the model (eq. 1) to guide the intuition, and then generalize to the full system. A number of different strategies for performing such reductions have been proposed [20, 35, 36], all of which could be equivalently employed. Our analysis relied on straightforward Poincaré mapping and fast-slow subsystem decomposition [25, 35].

Since ISI signatures are defined in terms of subsequent maxima in membrane potential traces, the Poincaré surface of section  $\Sigma$  had to be constructed in a way that the time between crossings corresponded to intermaxima intervals for the  $V$  variable. Such requirement was satisfied by adopting the surface defined by  $\dot{V} = 0$  (see Fig. 1B for a schematic representation of  $\Sigma$  and a trajectory for the full model).

In the slow-fast decomposition,  $m_{\text{KM}}$  is treated as a control parameter for the fast subsystem. We built unidimensional maps characterizing the full dynamics by gridding the interval



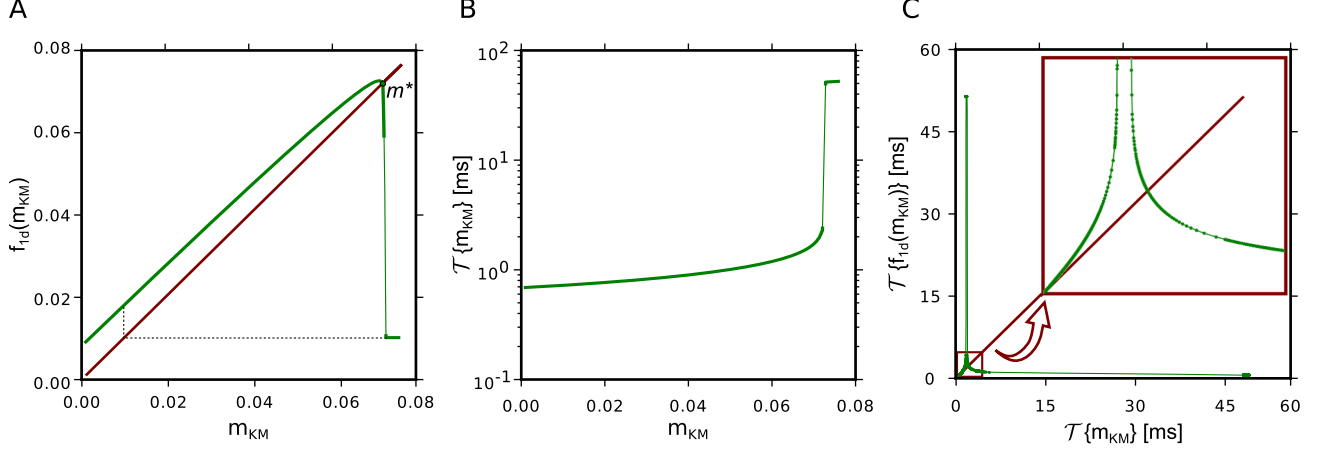


FIG. 3. One dimensional reduction of the dynamics. Panel A: discrete dynamics  $f_{1d}(m_{KM})$  of the slow variable. The highly-negative derivative section close to the fixed point  $m^*$  is of paramount importance in the suppression/addition of burstlets at the end of a burst, leading to complex ISI signatures. B: the observable  $\mathcal{T}\{m_{KM}\}$  coupled to the dynamics in A, that encodes the (full model) time elapsed in a  $f_{1d}(m_{KM})$  mapping. C: The ISI signature, defined in terms of the observable  $\mathcal{T}\{.\}$ . The thin lines connecting calculated points were added to guide the eye.

of  $m_{KM}$  values that supported limit cycles in the fast subsystem, and using intersections of  $\Sigma$  with these cycles as initial conditions for integrating the full system (eq. 1).

The discrete dynamics of  $m_{KM}$  in the intersection of the Poincaré surface of section  $\Sigma$  with the limit cycle manifold  $\mathcal{L}$  is depicted in Fig. 3A. The mapping  $f_{1d}(m_{KM})$  is the updated value of  $m_{KM}$  obtained by integrating the system along a cycle starting from the initial conditions described above, which provided us the (full model) time elapsed between each  $\Sigma \cap \mathcal{L}$  crossing. Hence, we were able to couple an “observable”  $\mathcal{T}\{m_{KM}\}$  to the dynamics, giving rise to the map in Fig. 3B. The ISI signature map is then straightforwardly defined in terms of this observable, as the pairs  $(\mathcal{T}\{m_{KM}\}, \mathcal{T}\{f_{1d}(m_{KM})\})$ , displayed in Fig. 3C.

### C. Mechanism of noise-induced irregularity

The apparent discontinuity in the mapping  $f_{1d}$  is instrumental in understanding irregularities in the number of spikes and total burst duration. Notice that the dynamics is not chaotic: the strongly dissipative quasi horizontal segment ( $m_{KM} \approx 0.07$ ) reinjects all trajectories into neighbouring points at the beginning of the spiking manifolds  $\mathcal{L}$ . Nevertheless it

is possible – due to noise – that trajectories reach the almost vertical region of  $f_{1d}$ , being mapped leftward and climbing back up the “tube”. Thus, the large negative derivative in  $f_{1d}$  amplifies microscopic noise, leading to irregular ISI patterns and burst durations even when the noiseless system supports only periodic bursting.

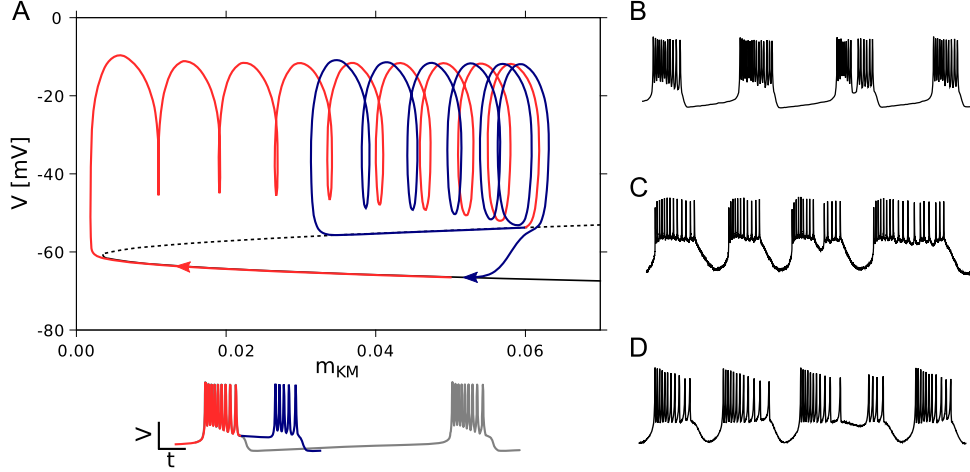


FIG. 4. Burstlets associated with canard trajectories. (A): The red part of the trajectory indicates the bursting “main sequence”, with the flux evolving through the spiking manifold  $\mathcal{L}$ . This particular trajectory does not fall directly to the stable part of the equilibria manifold (black curve) after  $\mathcal{L}$  loses stability in the homoclinic bifurcation. Instead, it glides along the unstable (saddle) branch of  $\mathcal{E}$  (dashed curve) for some time (blue part of trajectory), until being reinjected into  $\mathcal{L}$ , thus generating a burstlet. The bottom traces represent the timecourse of the burstlet trajectory, superimposed with a regular (gray) one. (B, C, D): burstlets in the stochastic Nap-Kd-KM model, a biological PD neuron and the stochastic Hindmarsh-Rose model, respectively.

Focusing back on the full model, it is possible to determine the origin of the abrupt, though continuous, change in  $f_{1d}$  after the fixed point  $m^*$ . There is an ensemble of states close to the end of the spiking manifold  $\mathcal{L}$  that, when evolving towards hyperpolarization, follow the saddle branch of the equilibrium manifold  $\mathcal{E}$  – as depicted in Fig. 4A – and are eventually reinjected into the spiking manifold  $\mathcal{L}$ . In the membrane potential timeseries, such reinjections would be reflected as prolongation of bursts by addition of spikes or “burstlets”: clusters of spikes appended to a bursting trajectory, after a hyperpolarization smaller than the typical interburst hyperpolarization. Examples of such burstlets can be seen in Fig. 4(B,C,D).

Trajectories that follow unstable structures such as the middle branch of  $\mathcal{E}$  are called *canards* [37, 38]. Note that these reinjections into  $\mathcal{L}$  can take place at any  $m_{\text{KM}}$  value up to the vicinity of the saddle-node bifurcation (see Fig. 5), depending on how long the trajectory follows the saddle branch. It is precisely this set of canard orbits that gives rise to the “dynamical skeleton” of ISI signatures, the deterministic substrate that is populated when noise is added to the model.

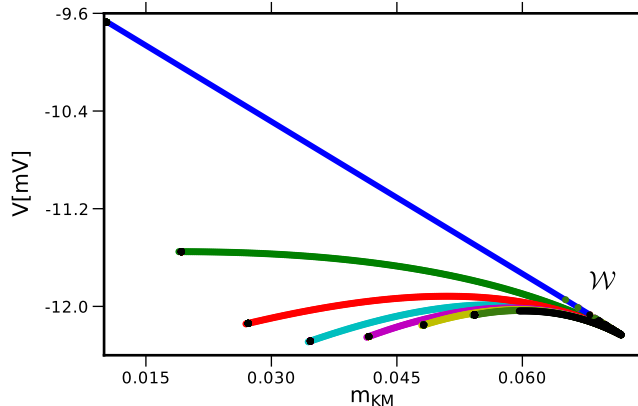


FIG. 5. Projection of  $\Sigma$  crossings into the  $m_{\text{KM}}V$  plane, for initial conditions close to the branch of saddles of the fast subsystem (segment of  $\mathcal{E}$  between SN and S-H in Fig. 1). As expected, it joins the extremes of the 9-spike periodic orbit of the unperturbed model at the endpoints of each curve. Other colours indicate further iterates of the blue line. The emerging wing-shaped structure is called  $\mathcal{W}$ .

#### D. Skeleton of the ISI signature map for the full model

Let  $f$  be the discrete dynamics on  $\Sigma$ , i.e. it generates a sequence of  $\Sigma$  crossings according to the full model dynamics, analogously to  $f_{1d}$  for the reduced model. Let  $\mathcal{T}$  be the time elapsed between two subsequent  $\Sigma$  crossings, analogously to  $\mathcal{T}$  for the unidimensional case. In order to unearth the skeleton, we take initial conditions over the unstable separatrices (approximated through the eigenvector corresponding to a positive eigenvalue) of a set of saddle points spanning the middle branch of  $\mathcal{E}$ , and integrate the full system until the first  $\Sigma$  crossing. These crossings give rise to the blue curve in Fig. 5. Subsequent iterations of this curve (each iteration is plotted with a different color in Fig. 5, and corresponds to integrating each point until the next  $\Sigma$  crossing) give rise to a flabellate structure  $\mathcal{W}$  in  $\Sigma$ .

The ISI signature skeleton is finally obtained as the  $(\mathcal{T}\{P\}, \mathcal{T}\{f(P)\})$  pairs for all points  $P$  in this structure, as shown in Fig. 6.

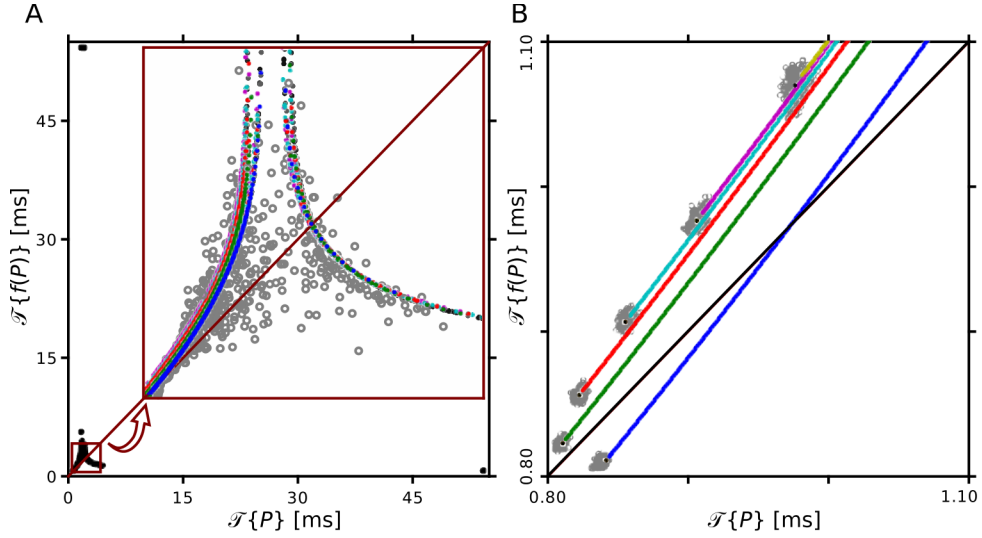


FIG. 6. Signature skeletons (filled circles):  $(\mathcal{T}\{P\}, \mathcal{T}\{f(P)\})$  pairs for points  $P$  in the flabellate structure  $\mathcal{W}$  of Fig. 5. The generated “infrastructure” is only accessible by the system through the addition of noise, given the strongly attractive character of the periodic bursting orbit. The unfilled grey points correspond to a signature generated by simulating the stochastic model. Panel B depicts the cluster generation mechanism for the first ISIs in a burst, along the deterministic scaffolding (coloured curves).

Fig. 7 represents the dynamics in  $\Sigma$  projected onto the  $m_{\text{KM}}V$  plane, with the addition of first return isochrons. An isochron is a subset of  $\Sigma$  with constant return time. In Fig. 7, a colour was assigned to each isochrone. The origin of the hook-shaped structure (“kink”) for the smallest ISI in the experimental signatures (Fig. 2-AB2, black-blue-green sequence) is elucidated by noticing that noise tends to spread crossings across isochrons. This way, two ISI in different positions along the burst are similar, leading to vertically stacked clusters in the  $(\mathcal{T}\{P\}, \mathcal{T}\{f(P)\})$  (signature) map.

### E. Simulation of ISI map signatures

The integration of the full (noisy) model (eqs. 1 and 2), in addition to a simple threshold ( $-30\text{mV}$ ) spike detection, leads to the ISI signature map in Fig. 8. This map qualitatively reproduces the structure of the ISI signature of biological neurons (Fig. 2), including fine

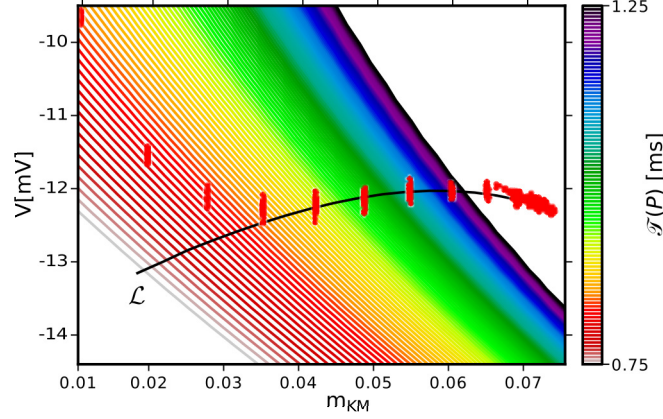


FIG. 7. Isochrons of return time to  $\Sigma$ . Long times (blank areas) have been discarded to increase readability. The black curve is the intersection of the surface of section  $\Sigma$  with the fast subsystem limit cycle manifold  $\mathcal{L}$ , corresponding to intraburst spiking. Red dots correspond to  $\Sigma$  crossings of an integrated trajectory of the full noisy model (equations 1 and 2). Noise tends to spread the crossing points across isochrons, so that spikes of different positions in a burst give rise to similar ISIs – generating “kinks” in the signature.

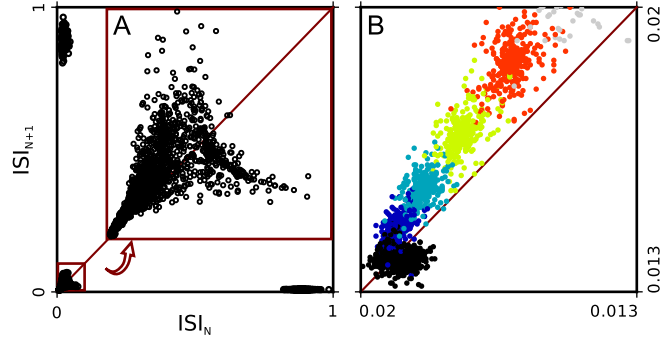


FIG. 8. ISI signature generated by the model of a square-wave burster neuron with channel noise (eqs. 1 and 2). Scaling of plots and point colors as in Fig. 2.

details such as the “kink” in the low ISI main sequence, as well as the variability in both number of spikes and interburst intervals (reflected in the diffusiveness at the end of the main sequence and the extent of the isolated high-ISI arms). All of these features can be traced back to an underlying deterministic scaffolding, so that the role of noise is to induce transient dynamics exposing this infrastructure. Note also that the qualitative resemblance between model and biological ISI maps was obtained without special tuning of model parameters. Similar structures were also obtained by adding noise to either pre-Bötzinger or Hindmarsh-

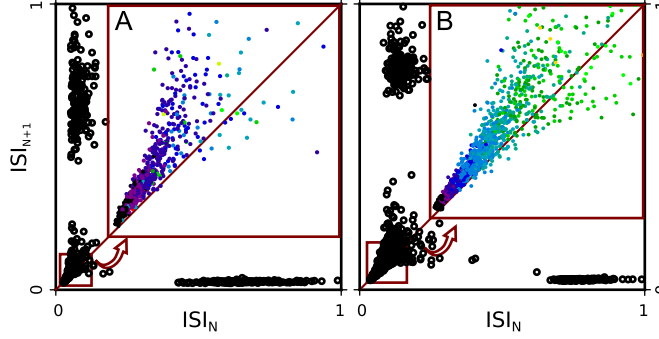


FIG. 9. (left): Signature generated by the pre-Bötzinger neuron model with conductance noise; (right): Signature generated by the Hindmarsh-Rose neuron model with current noise. Conventions as in Figs. 2 and 8.

Rose model neurons (Fig. 9), suggesting that similar mechanisms may be at work in these cases also.

#### IV. DISCUSSION

The presented mechanism accounts for the generation of irregular bursting traces with complex signatures, in terms of a low-dimensional conductance-based model and a macroscopic approximation of stochastic gating noise. Noise plays a crucial role in the mechanism: although the deterministic scaffolding of the model (its “skeleton”) can support complex behaviour, this dynamical richness is usually suppressed by the dissipative character of the periodic bursting or tonic spiking orbits. Noise, however, unveils the transient dynamics, giving flesh to the skeleton and generating the ISI signature patterns characteristic of biological neurons. Let  $\Sigma$  be the hypersurface defined by  $\dot{V} = 0$ , which will be  $[n-1]$ -dimensional in a  $n$ -dimensional conductance-based model. The set of intersections of  $\Sigma$  with the unstable  $([n-1]d)$  manifolds of the saddles in the middle branch  $([n-2]d)$  and its iterates defines the flabellate structure  $\mathcal{W}$ . Skeletons are the image of the ISI return map transformation applied to  $\mathcal{W}$ .

We emphasize the robustness of the skeleton to parameter fluctuations: since it is inherently tied to the bifurcation structure of the model, its general features persist even through bursting-tonic transitions (associated with the gain of stability of the fixed point in the unidimensional map  $f_{1d}$ ). Signatures essentially will remain the same for scenarios in which

bursting is induced by noise (the noiseless system otherwise spiking tonically) [24]. That seems indeed to be the case for the PD neuron (Fig. 2B), given the presence of very long (more than 100 spikes) bursts and comparatively shorter hyperpolarization periods.

Irregular activity in neuronal models has been associated with the presence of deterministic chaos [39–41]. Nevertheless, the main cause of irregularities in our model is the amplification of stochastic phenomena by the transient dynamics. Structures defined by such dynamics persist even for parameter regimes that do not support chaotic attractors. Noise-induced chaos [42] – where the neighbourhood of non-attracting hyperbolic sets is visited due to perturbations – could be present, as chaotic saddles can arise in spike-adding transitions as shown in [19]. This would, however, involve fine tuning of parameters and might prove too delicate to detect [43] with large noise intensities such as those needed, seemingly, to simulate biological results. Similar considerations may apply also to “stochastic chaos” associated with D-type stochastic bifurcations [44].

Bursting activity can be generated through several distinct geometric mechanisms [23] in addition to the saddle-node/homoclinic behavior studied here. Using the proposed geometrical framework, general features of the dispersion of ISI pairs in neuronal signature maps can be predicted. In particular, the burstlet generation mechanism via canard trajectories will require bursting scenarios involving a saddle middle branch.

As different levels of noise are added to the model, there is a scaling of ISI cluster dispersion (data not shown). This provides a possible method of estimating the dynamical noise level in time series analysis of real neurons. We also point out that the burstlet definition and description can be used to improve burst alignment algorithms [45], through separating bursts into a “main sequence” followed by irregular burstlets.

## ACKNOWLEDGMENTS

Financial support from the Brazilian agencies *Fundação de Amparo à Pesquisa do Estado de São Paulo* (FAPESP), *Coordenação de Aperfeiçoamento de Pessoal de Nível Superior* (CAPES) and *Conselho Nacional de Desenvolvimento Científico e Tecnológico* (CNPQ) is gratefully acknowledged. RCE was supported by a grant from *National Science Foundation*.

We thank Geoffrey Evans for useful feedback on the manuscript.

---

- [1] A. Szücs, R. D. Pinto, M. I. Rabinovich, H. D. I. Abarbanel, and A. I. Selverston, *Journal of Neurophysiology* **89**, 1363 (2003).
- [2] A. Szücs, H. D. I. Abarbanel, M. I. Rabinovich, and A. I. Selverston, *The European Journal of Neuroscience* **21**, 763 (2005).
- [3] G. M. Zeck and R. H. Masland, *The European Journal of Neuroscience* **26**, 367 (2007).
- [4] L. Garcia, G. D'Alessandro, P.-O. Fernagut, B. Bioulac, and C. Hammond, *Journal of Neurophysiology* **94**, 3662 (2005).
- [5] L. Brochini, P. V. Carelli, and R. D. Pinto, *The Journal of Neuroscience* **31**, 12297 (2011).
- [6] Y. Zhurov and V. Brezina, *The Journal of Neuroscience* **26**, 7056 (2006).
- [7] J. Lisman, *Trends in Neurosciences* **20**, 38 (1997).
- [8] B. Doiron, M. J. Chacron, L. Maler, A. Longtin, and J. Bastian, *Nature* **421**, 539 (2003).
- [9] E. M. Izhikevich, N. S. Desai, E. C. Walcott, and F. C. Hoppensteadt, *Trends in Neurosciences* **26**, 161 (2003).
- [10] A.-M. M. Oswald, M. J. Chacron, B. Doiron, J. Bastian, and L. Maler, *The Journal of Neuroscience* **24**, 4351 (2004).
- [11] F. de Borja Rodríguez, R. Latorre, and P. Varona, *Artificial Neural Networks — ICANN 2002*, edited by J. R. Dorronsoro, *Lecture Notes in Computer Science*, Vol. 2415 (Springer Berlin Heidelberg, Berlin, Heidelberg, 2002) pp. 167–173.
- [12] R. Latorre, F. de Borja Rodríguez, and P. Varona, *Biological Cybernetics* **95**, 169 (2006).
- [13] A. Tristan, F. De Borja Rodriguez, E. Serrano, and P. Varona, *Neurocomputing* **58-60**, 41 (2004).
- [14] R. C. Elson, R. Huerta, H. D. I. Abarbanel, M. I. Rabinovich, and A. I. Selverston, *Journal of Neurophysiology* **82**, 115 (1999).
- [15] A. I. Selverston, M. I. Rabinovich, H. D. I. Abarbanel, R. Elson, A. Szücs, R. D. Pinto, R. Huerta, and P. Varona, *Journal of Physiology, Paris* **94**, 357 (2000).
- [16] A. A. Prinz, C. P. Billimoria, and E. Marder, *Journal of Neurophysiology* **90**, 3998 (2003).
- [17] J. Guckenheimer and R. A. Oliva, *Journal of Applied Dynamical Systems* **1**, 105 (2002).
- [18] A. L. Shilnikov, R. L. Calabrese, and G. Cymbalyuk, *Physical Review E* **71**, 056214 (2005).



- [19] D. Terman, SIAM Journal on Applied Mathematics **51**, 1418 (1991).
- [20] G. Medvedev, Physical Review Letters **97**, 1 (2006).
- [21] J. P. Miller and A. I. Selverston, Journal of Neurophysiology **48**, 1416 (1982).
- [22] T. Bal, F. Nagy, and M. Moulins, Journal of Comparative Physiology A **163**, 715 (1988).
- [23] E. M. Izhikevich, International Journal of Bifurcations and Chaos **10**, 1171 (2000).
- [24] P. Hitczenko and G. Medvedev, SIAM Journal on Applied Mathematics **69**, 1359 (2009).
- [25] N. Fenichel, Journal of Differential Equations **31**, 53 (1979).
- [26] T. R. Chay and J. Keizer, Biophysical Journal **42**, 181 (1983).
- [27] R. J. Butera, J. Rinzel, and J. C. Smith, Journal of Neurophysiology **82**, 382 (1999).
- [28] J. Best, A. Borisjuk, J. Rubin, D. Terman, and M. Wechselberger, SIAM Journal on Applied Dynamical Systems **4**, 1107 (2005).
- [29] D. Golomb, C. Yue, and Y. Yaari, Journal of Neurophysiology **96**, 1912 (2006).
- [30] J. L. Hindmarsh and R. M. Rose, Proceedings of the Royal Society of London. Series B. **221**, 87 (1984).
- [31] P. F. Rowat and R. C. Elson, Journal of Computational Neuroscience **16**, 87 (2004).
- [32] J. H. Goldwyn and E. Shea-Brown, PLoS Computational Biology **7**, e1002247 (2011).
- [33] R. F. Fox, Biophysical Journal **72**, 2068 (1997).
- [34] P. Kloeden and E. Platen, *Numerical Solution of Stochastic Differential Equations* (Springer-Verlag, Berlin, 1992).
- [35] G. Medvedev, Physica D: Nonlinear Phenomena **202**, 37 (2005).
- [36] P. Channell Jr, G. S. Cymbalyuk, and A. L. Shilnikov, Neurocomputing **70**, 2107 (2007).
- [37] H. G. Rotstein, S. Coombes, and A. M. Gheorghe, SIAM Journal on Applied Dynamical Systems **11**, 135 (2012).
- [38] J. Burke, M. Desroches, A. M. Barry, T. J. Kaper, and M. A. Kramer, Journal of Mathematical Neuroscience **2**, 3 (2012).
- [39] M. Falcke, R. Huerta, M. I. Rabinovich, H. D. Abarbanel, R. C. Elson, and A. I. Selverston, Biological Cybernetics **82**, 517 (2000).
- [40] P. V. Carelli, M. B. Reyes, J. C. Sartorelli, and R. D. Pinto, Journal of Neurophysiology **94**, 1169 (2005).
- [41] P. Channell Jr, I. Fuwape, A. B. Neiman, and A. L. Shilnikov, Journal of Computational Neuroscience **27**, 527 (2009).

- [42] Z. Liu, Y. C. Lai, L. Billings, and I. Schwartz, “Transition to Chaos in Continuous-Time Random Dynamical Systems,” (2002).
- [43] J. B. Gao, C. C. Chen, S. K. Hwang, and J. M. Liu, International Journal Of Modern Physics **13**, 3283 (1999).
- [44] E. K. Kosmidis and K. Pakdaman, International Journal of Bifurcation and Chaos **16**, 395 (2006).
- [45] L. F. Lago-Fernández, A. Szücs, and P. Varona, Neural Computation **21**, 973 (2009).